

Computational investigation of formation enthalpies and phase stability for rare earth oxyphosphates

Edric X. Wang^{a,b}, Ligen Wang^a, Qi-Jun Hong^{a,*}

^a School for Engineering of Transport, Energy and Matter, Arizona State University, Tempe, AZ 85287, USA

^b Department of Materials Science and Engineering, University of Illinois at Urbana-Champaign, Urbana, IL 61801, USA

Abstract

Rare earth phosphates have garnered significant interest due to their versatile properties, including high chemical stability, thermal resistance, luminescence, and the ability to adopt various crystalline structures. Density functional theory (DFT)-based ab initio methods have become essential tools for complementing experimental studies. In this paper, we performed DFT calculations on rare earth (RE; here considered as lanthanides + Y) oxyphosphates to examine their formation enthalpies and phase stability. The calculations were conducted using the GGA-PBE and r2SCAN exchange-correlation functionals. Our results indicate that both functionals predict similar phase stabilities for REPO₄ and RE₃PO₇. However, the r2SCAN functional provides significantly more accurate formation enthalpies for the monazite and xenotime REPO₄, aligning closely with experimental data. Furthermore, the inclusion of lattice vibrational entropy enhances the free energy predictions, leading to improved agreement with experimental observations on phase stability.

Keywords: *Density functional theory calculations, Rare earth phosphates, Formation enthalpies, Thermodynamic stability, Vibrational entropy*

1. Introduction

Rare earth orthophosphates, such as monazite and xenotime, are among the most refractory minerals known, with extensive applications ranging from laser hosts to actinide immobilization matrices. In contrast, their synthetic counterparts, rare earth oxyphosphates (REOPs), have been largely overlooked since their discovery nearly half a century ago [1], despite their potential significance. REOPs are characterized by the general formula $(\text{RE}_2\text{O}_3)_x\text{RE}(\text{PO}_4)$, with RE/P ratios of 7:3, 3:1, 4:1, and 5:1. Rare earth oxyphosphates have been successfully synthesized using methods such as co-precipitation followed by high-temperature annealing, and laser melting of REPO_4 [2]. Both experimental and computational approaches are being used to explore the structures and thermodynamic and physical properties of REOPs [1-11].

Rare earth oxyphosphates are characterized by their unique structural, optical, and thermal properties, making them valuable in a wide range of scientific and industrial applications. The interest in rare earth oxyphosphates stems from their high chemical stability, thermal resistance, luminescent capabilities, and ability to form a variety of crystalline structures, which can be tailored for specific uses in catalysis, luminescence, environmental science, material science, and biomedicine [3-9].

Computational materials science has made significant progress over the past few decades, largely driven by advancements in computational power and the development of ab initio methods, such as density functional theory (DFT) [12-14]. These methods allow researchers to simulate the atomic-scale behavior of materials, providing insights into their chemical and physical properties. This computational approach complements experimental techniques, enabling the exploration of atomic mechanisms responsible for material performance, such as stability, phase transitions, and reaction pathways. By modeling atomic interactions with increasing accuracy, computational methods have substantially expanded our understanding of materials, aiding in the design of more efficient and advanced materials across various applications [14].

In this study, we conducted a computational analysis of the formation enthalpies and phase stability of rare earth phosphates. Using density functional theory with the GGA-PBE

[15] and r2SCAN [16] exchange-correlation functionals, we found that both functionals predicted similar phase stabilities for REPO_4 and RE_3PO_7 . However, the r2SCAN functional yielded significantly more accurate formation enthalpies for monazite and xenotime REPO_4 , closely matching experimental results. Thermal effects, such as thermal expansion and lattice vibrational entropy, were also calculated to determine free energy, which improved phase stability predictions and enhanced agreement with experimental observations.

2. Computational methods

The calculations are performed within the framework of DFT using the Vienna Ab-initio Simulation Package (VASP) [17,18]. Projector augmented wave (PAW) pseudopotentials [19] are employed to describe the interactions between ions and valence electrons. For the lanthanides Ce–Lu, pseudopotentials with a specific valence state of 3 are used, where the number of f-electrons frozen in the core is equal to the total number of valence electrons minus the formal valency [20]. For example, according to the periodic table, Sm has 8 valence electrons in total—6 f-electrons and 2 s-electrons. In most compounds, Sm typically exhibits a valency of 3, meaning that when the Sm₃ pseudopotential is generated, 5 f-electrons are treated as core electrons [20]. In density functional theory calculations, the generalized gradient approximation (GGA) for the exchange-correlation functional is widely used, offering a balance between computational efficiency and accuracy. Recent large-scale benchmarking of approximately 6,000 solid materials has shown that the r2SCAN exchange-correlation functional delivers both high numerical efficiency and accuracy, making it a preferred choice for many applications [21,22]. Specifically, r2SCAN provides more accurate formation enthalpies than GGA, the SCAN [23] and PBEsol [24] functionals for materials with both strong and weak bonding. In this work, we used the r2SCAN functional and compared its results with those obtained using the GGA-PBE functional. The plane wave basis set had an energy cutoff of 520 eV. The Brillouin zone was sampled with k-point meshes [25] that were similar in structure but denser than those used in the Materials Project database [11]. The total energy convergence was carefully tested with respect to the density of the k-point grid. Supercell parameters and atomic positions were optimized until the total energy

converged within 10^{-5} eV, and atomic forces were minimized to below 0.02 eV/Å.

The enthalpies of formation of monazite and xenotime REPO_4 are calculated assuming the reaction: $\frac{1}{2}\text{RE}_2\text{O}_3 + \frac{1}{2}\text{P}_2\text{O}_5 \rightarrow \text{REPO}_4$. The formation enthalpy for REPO_4 with respect to RE_2O_3 and P_2O_5 oxides is defined as

$$\Delta E_f^{ox} = E_{\text{tot}}(\text{REPO}_4) - \frac{1}{2}E_{\text{tot}}(\text{RE}_2\text{O}_3) - \frac{1}{2}E_{\text{tot}}(\text{P}_2\text{O}_5), \quad (1)$$

where $E_{\text{tot}}(\text{REPO}_4)$, $E_{\text{tot}}(\text{RE}_2\text{O}_3)$, and $E_{\text{tot}}(\text{P}_2\text{O}_5)$ are the total energies for the bulk solid phases.

Stability with respect to phase separation can be assessed using the convex hull formalism [26]. To assess the (in)stability of RE_3PO_7 phase, the reaction energy for forming RE_3PO_7 from the linear combination of neighbors (RE_2O_3 and REPO_4) in composition space is defined as:

$$\Delta E_f = E_{\text{tot}}(\text{RE}_3\text{PO}_7) - E_{\text{tot}}(\text{RE}_2\text{O}_3) - E_{\text{tot}}(\text{REPO}_4), \quad (2)$$

where $E_{\text{tot}}(\text{RE}_3\text{PO}_7)$, $E_{\text{tot}}(\text{RE}_2\text{O}_3)$, and $E_{\text{tot}}(\text{REPO}_4)$ are the total energies for RE_3PO_7 , RE_2O_3 , and REPO_4 , respectively. For an unstable compound that lies above the convex hull, $\Delta E_f > 0$, whereas for a stable compound that lies on or below the convex hull, $\Delta E_f \leq 0$.

3. Results and discussions

3.1 Structure and energetics of rare earth sesquioxides

Rare earth sesquioxides exhibit various polymorphs across different temperature ranges, including the cubic (C), monoclinic (B), and hexagonal (A) phases at low temperatures, as well as the high-temperature hexagonal (H) and cubic (X) phases [27,28]. Table 1 presents the calculated energies for RE oxides in the low-temperature A, B, and C structures. For all sesquioxides, the C phase has the lowest total energy, establishing it as the ground state based on GGA-PBE calculations. Using the r2SCAN exchange-correlation functional, the C phase remains stable for all RE_2O_3 compounds except La_2O_3 and Ce_2O_3 . As shown in Table 1, the A and C phases of La_2O_3 , Ce_2O_3 , and Pr_2O_3 are nearly isoenergetic. These predictions using the r2SCAN exchange-correlation functional align more closely with experimental observations, as the light rare earth oxides— La_2O_3 , Ce_2O_3 , Pr_2O_3 , and Nd_2O_3 —are known to be most stable

in the hexagonal A-type structure [27,28]. Table 2 and Fig. 1 present the optimized structural parameters and molar volumes for the C-type RE₂O₃ oxides. For comparison, experimental values obtained from X-ray measurements and previously calculated results [29] are also included. The lattice constants for all RE oxides, except Ce₂O₃, are accurately predicted by both the GGA-PBE and r2SCAN functionals, with errors less than 1% relative to experimental values. For Ce₂O₃, the prediction errors are approximately 2.7% (GGA-PBE) and 2.5% (r2SCAN), respectively. The discrepancy between the calculated and experimental lattice constants for Ce₂O₃ may result from the presence of the Ce⁴⁺-related phase and/or intermediate phases between Ce₂O₃ and CeO₂ in the experimental samples [30,31]. The r2SCAN functional systematically predicts smaller lattice constants than the GGA-PBE functional. Compared to experimental data, r2SCAN provides better accuracy for material systems with larger rare earth elements (Y and those earlier than Eu) but less accuracy for oxides with smaller rare earth metals (Gd through Lu). Our GGA-PBE results for both phase stability and lattice constants agree well with previously reported GGA-PBE calculations [29]. Together, these structural parameters and the formation enthalpy results presented below suggest that the r2SCAN exchange-correlation functional offers a more accurate description of rare earth oxides and oxyphosphates than the GGA-PBE functional.

Table 1. Total energies for RE₂O₃ (eV/formula unit) calculated by the GGA-PBE and r2SCAN functionals.

	<u>GGA-PBE</u>			<u>r2SCAN</u>		
	A-type	B-type	C-type	A-type	B-type	C-type
La ₂ O ₃	-41.825	-41.799	-41.948	-96.057	-96.006	-96.051
Ce ₂ O ₃	-40.586	-40.572	-40.697	-94.517	-94.481	-94.505
Pr ₂ O ₃	-40.827	-40.824	-40.955	-94.718	-94.693	-94.725
Nd ₂ O ₃	-41.004	-41.013	-41.154	-95.025	-95.011	-95.054
Sm ₂ O ₃	-41.217	-41.253	-41.415	-96.041	-96.056	-96.125
Eu ₂ O ₃	-41.368	-41.417	-41.590	-97.095	-97.162	-97.258
Gd ₂ O ₃	-41.522	-41.587	-41.775	-98.318	-98.370	-98.476
Tb ₂ O ₃	-41.589	-41.670	-41.872	-99.679	-99.748	-99.873
Dy ₂ O ₃	-41.636	-41.734	-41.949	-101.286	-101.374	-101.517
Y ₂ O ₃	-45.411	-45.529	-45.771	-77.757	-77.868	-78.042

Ho ₂ O ₃	-41.677	-41.790	-42.019	-103.161	-103.270	-103.431
Er ₂ O ₃	-41.720	-41.851	-42.093	-105.356	-105.482	-105.655
Tm ₂ O ₃	-41.796	-41.944	-42.199	-107.927	-108.073	-108.269
Yb ₂ O ₃	-41.829	-41.995	-42.267	-110.841	-111.009	-111.222
Lu ₂ O ₃	-41.859	-42.041	-42.326	-113.951	-114.139	-114.373

Table 2. Structural parameters for cubic C-type RE₂O₃ (volume in Å³/formula unit). The measured structural parameters taken from Ref. [29] were gathered from various experimental studies.

	<u>Calculated (this work)</u>				<u>Calculated (Ref. [29])</u>		<u>Measured</u>	
	<u>GGA-PBE</u>		<u>r2SCAN</u>		<u>GGA-PBE</u>		<u>a (Å)</u>	<u>V (Å³)</u>
	<u>a (Å)</u>	<u>V (Å³)</u>	<u>a (Å)</u>	<u>V (Å³)</u>	<u>a (Å)</u>	<u>V (Å³)</u>		
La ₂ O ₃	11.397	92.54	11.364	91.73	11.387	92.29	-	-
Ce ₂ O ₃	11.409	92.82	11.377	92.03	11.414	92.94	11.111	85.73
Pr ₂ O ₃	11.278	89.66	11.248	88.94	11.290	89.94	-	-
Nd ₂ O ₃	11.173	87.19	11.130	86.16	11.178	87.30	-	-
Sm ₂ O ₃	10.989	82.93	10.943	81.91	10.998	83.14	10.930	81.61
Eu ₂ O ₃	10.899	80.91	10.844	79.70	-	-	-	-
Gd ₂ O ₃	10.809	78.92	10.747	77.58	10.819	79.16	10.790	78.51
Tb ₂ O ₃	10.736	77.34	10.669	75.91	10.744	77.50	10.729	77.10
Dy ₂ O ₃	10.665	75.82	10.598	74.39	10.675	76.02	10.670	75.92
Y ₂ O ₃	10.655	75.60	10.611	74.67	10.701	76.58	10.596	74.36
Ho ₂ O ₃	10.602	74.49	10.527	72.92	10.609	74.63	10.580	74.02
Er ₂ O ₃	10.544	73.27	10.462	71.56	10.544	73.26	10.548	73.35
Tm ₂ O ₃	10.474	71.81	10.391	70.12	10.472	71.77	10.480	71.94
Yb ₂ O ₃	10.414	70.59	10.332	68.94	-	-	-	-
Lu ₂ O ₃	10.354	69.38	10.267	67.64	-	-	-	-

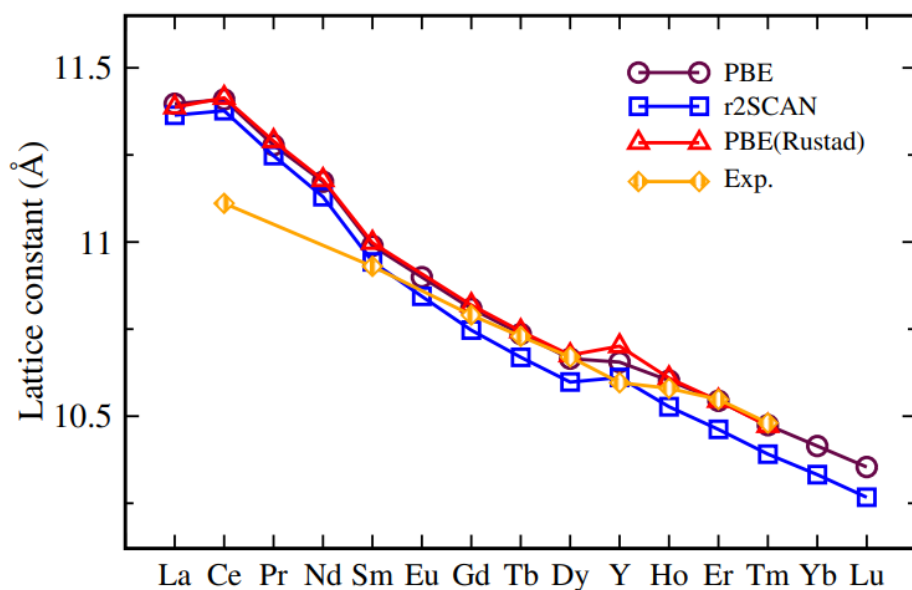


Fig. 1. Calculated lattice constant results for the C-type RE_2O_3 oxides, together with the experimental and previously reported theoretical values (Ref. [29]).

3.2 Phase stability and formation enthalpies of REPO_4

Rare earth phosphates, REPO_4 , naturally occur in the monazite and xenotime phases. The formation enthalpies of rare earth orthophosphates from their oxides have been studied both experimentally [10] and computationally [29,32-34]. Previous studies identified two key issues when using density functional theory (DFT) to calculate the energetics of rare earth orthophosphates. First, DFT calculations inaccurately predict the xenotime phase to be more stable than the monazite phase for EuPO_4 and SmPO_4 [29]. For NdPO_4 , prior DFT calculations with the GGA-PBE functional showed the monazite and xenotime structures to be nearly isoenergetic, with the monazite structure having slightly lower energy [29]. The second issue is that the calculated formation enthalpies are consistently less exothermic by approximately 40 kJ/mol compared to measured values [29,32-34]. This discrepancy is attributed to challenges in accurately describing phosphorus pentoxide and P–O bonds within DFT [32,34]. Here, formation enthalpy calculations for rare earth orthophosphates were performed using both the PBE and r2SCAN functionals. The r2SCAN functional has been shown to provide more accurate formation enthalpies across various materials, including oxides, rare earths, transition metal intermetallics and compounds, as well as materials with strong and weak bonding [21,22]. Thus, it is expected to deliver improved performance for

rare earth orthophosphates. One advantage of theoretical calculations is the ability to investigate structures that have not been observed experimentally, such as xenotime LaPO_4 and monazite LuPO_4 . Our calculations cover all monazite and xenotime REPO_4 structures, including those not experimentally observed. Formation enthalpies are calculated based on the reaction in Eq. (1).

Table 3 presents the total energies (E^M and E^X) and energy differences (ΔE^{M-X}) between the monazite and xenotime structures, along with previously reported results [29]. Subtle differences in total energies compared to prior calculations can be attributed to variations in computational parameters, despite both studies using the GGA-PBE exchange-correlation functional. The ΔE^{M-X} values from both GGA-PBE calculations show excellent agreement. However, the ΔE^{M-X} values obtained using the r2SCAN exchange-correlation functional differ notably from the GGA-PBE values, showing a stronger preference for the monazite structure. Importantly, both GGA-PBE and r2SCAN functionals predict the same phase stability trends: the monazite phase is more stable for La-, Ce-, Pr-, and Nd-orthophosphates, whereas the xenotime phase is more stable for all other orthophosphates (Sm–Lu and Y), as shown in Table 3 and Fig. 2. This prediction, however, appears inconsistent with experimental observations [10,35]. As discussed below, the monazite structure for certain orthophosphates (SmPO_4 , EuPO_4 , and GdPO_4) with small positive ΔE^{M-X} values becomes stable at finite temperatures.

The calculated formation enthalpies are presented in Fig. 3 and Table 4, alongside experimental formation enthalpies (ΔH_f^{ox} at 298 K) [10] for comparison. We used metastable hexagonal P_2O_5 (R3c, 161) in our formation enthalpy calculations to match the reference phase used in the experimental formation enthalpy measurements by Ushakov et al. [10]. With the r2SCAN exchange-correlation functional, the h- P_2O_5 phase is 0.051 eV/atom higher in energy than the polymeric orthorhombic o'- P_2O_5 compound, consistent with the Materials Project (MP) database value [11] and greater than the energy difference of 0.022 eV/atom calculated using the GGA-PBE functional [29]. As shown in previous studies, GGA-PBE formation enthalpies tend to be less exothermic by approximately 40 kJ/mol relative to experimental $\Delta H_f^{ox}(298\text{K})$ values, while r2SCAN results have a notably smaller average

error (RMSE of 8.7 kJ/mol). The improvement in formation enthalpy accuracy with r2SCAN cannot be fully explained by the energy difference between h-P₂O₅ and o'-P₂O₅, indicating r2SCAN's overall effectiveness in providing more accurate formation enthalpies for rare earth orthophosphates. As found in previous DFT calculations [29,33,34], the largest errors for both GGA-PBE and r2SCAN functionals occur with monazite GdPO₄ and TbPO₄.

Table 3. Calculated energies (eV/formula unit) of REPO₄ in the monazite (M) and xenotime (X) structures

	Calculated (this work)						Calculated (Ref.[29])		
	GGA-PBE			r2SCAN			GGA-PBE		
	E^M	E^X	ΔE^{M-X}	E^M	E^X	ΔE^{M-X}	E^M	E^X	ΔE^{M-X}
LaPO ₄	-48.373	-48.250	-0.123	-82.615	-82.373	-0.242	-48.337	-48.215	-0.122
CePO ₄	-47.850	-47.723	-0.127	-81.950	-81.709	-0.240	-47.805	-47.679	-0.126
PrPO ₄	-47.879	-47.814	-0.065	-81.961	-81.788	-0.173	-47.843	-47.779	-0.064
NdPO ₄	-47.884	-47.876	-0.008	-82.029	-81.919	-0.110	-47.854	-47.846	-0.008
SmPO ₄	-47.842	-47.936	0.094	-82.379	-82.385	0.007	-47.835	-47.923	0.088
EuPO ₄	-47.844	-47.991	0.148	-82.826	-82.906	0.080	-	-	-
GdPO ₄	-47.838	-48.037	0.199	-83.344	-83.478	0.134	-47.819	-48.013	0.194
TbPO ₄	-47.803	-48.046	0.243	-83.949	-84.135	0.186	-47.788	-48.027	0.239
DyPO ₄	-47.759	-48.044	0.285	-84.677	-84.913	0.236	-	-48.025	-
YPO ₄	-49.622	-49.915	0.293	-72.922	-73.157	0.235	-	-49.760	-
HoPO ₄	-47.713	-48.039	0.326	-85.540	-85.824	0.284	-	-48.022	-
ErPO ₄	-47.675	-48.040	0.365	-86.571	-86.904	0.332	-	-48.031	-
TmPO ₄	-47.652	-48.060	0.408	-87.788	-88.174	0.386	-	-47.991	-
YbPO ₄	-47.604	-48.048	0.444	-89.190	-89.616	0.426	-	-	-
LuPO ₄	-47.544	-48.031	0.486	-90.652	-91.128	0.476	-	-	-

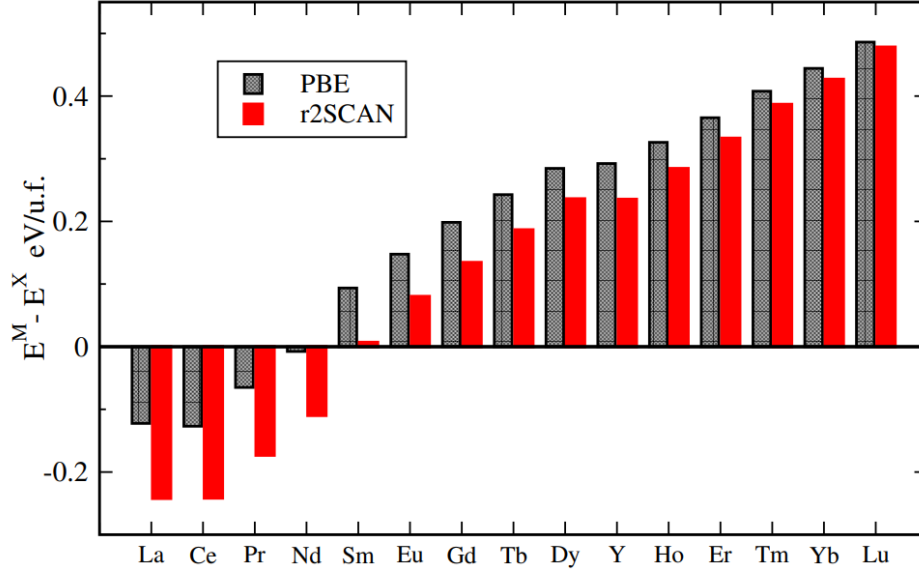


Fig. 2. Energy difference ΔE^{M-X} between the monazite and xenotime rare earth orthophosphates.

Table 4. Formation enthalpies ΔE_f^{ox} (kJ/mol) at 0K with respect to oxides for $REPO_4$ in the monazite (M) and xenotime (X) structures

	Measured	Calculated	$\Delta E_f^{ox}(0K)$	$\Delta E_f^{ox}(0K) - \Delta H_f^{ox}(298K)$	
	$\Delta H_f^{ox}(298K)$	GGA-PBE	r2SCAN	GGA-PBE	R2SCAN
LaPO ₄ (m)	-321.4	-279.4	-321.7	42.0	-0.3
LaPO ₄ (x)	-	-267.6	-298.6	-	-
CePO ₄ (m)	-317.2	-289.4	-331.7	27.8	-14.5
CePO ₄ (x)	-	-277.1	-309.1	-	-
PrPO ₄ (m)	-312.2	-279.7	-322.8	32.5	-10.6
PrPO ₄ (x)	-	-273.5	-306.1	-	-
NdPO ₄ (m)	-312.0	-270.6	-313.4	41.4	-1.4
NdPO ₄ (x)	-	-269.9	-302.8	-	-
SmPO ₄ (m)	-301.8	-254.0	-295.6	47.8	6.2
SmPO ₄ (x)	-	-263.0	-296.2	-	-
EuPO ₄ (m)	-286.8	-245.7	-284.1	41.1	2.7
EuPO ₄ (x)	-	-259.9	-291.8	-	-
GdPO ₄ (m)	-296.2	-236.2	-275.2	60.0	21.0
GdPO ₄ (x)	-	-255.4	-288.2	-	-
TbPO ₄ (m)	-283.5	-228.1	-266.2	55.4	17.3
TbPO ₄ (x)	-286.1	-251.6	-284.2	34.5	1.9

DyPO ₄ (m)	-	-220.2	-257.2	-	-
DyPO ₄ (x)	-283.9	-247.7	-279.9	36.2	4.0
YPO ₄ (m)	-	-215.6	-255.5	-	-
YPO ₄ (x)	-282.6	-243.8	-278.1	38.8	4.5
HoPO ₄ (m)	-	-212.4	-248.1	-	-
HoPO ₄ (x)	-278.8	-243.9	-275.5	34.9	3.3
ErPO ₄ (m)	-	-205.1	-240.3	-	-
ErPO ₄ (x)	-275.6	-240.4	-272.4	35.2	3.2
TmPO ₄ (m)	-	-197.8	-231.6	-	-
TmPO ₄ (x)	-268.0	-237.1	-268.9	30.9	-0.9
YbPO ₄ (m)	-	-189.9	-224.4	-	-
YbPO ₄ (x)	-269.6	-232.7	-265.5	36.9	4.1
LuPO ₄ (m)	-	-181.3	-213.5	-	-
LuPO ₄ (x)	-263.9	-228.2	-259.4	35.7	4.5
RMSE				40.3	8.7

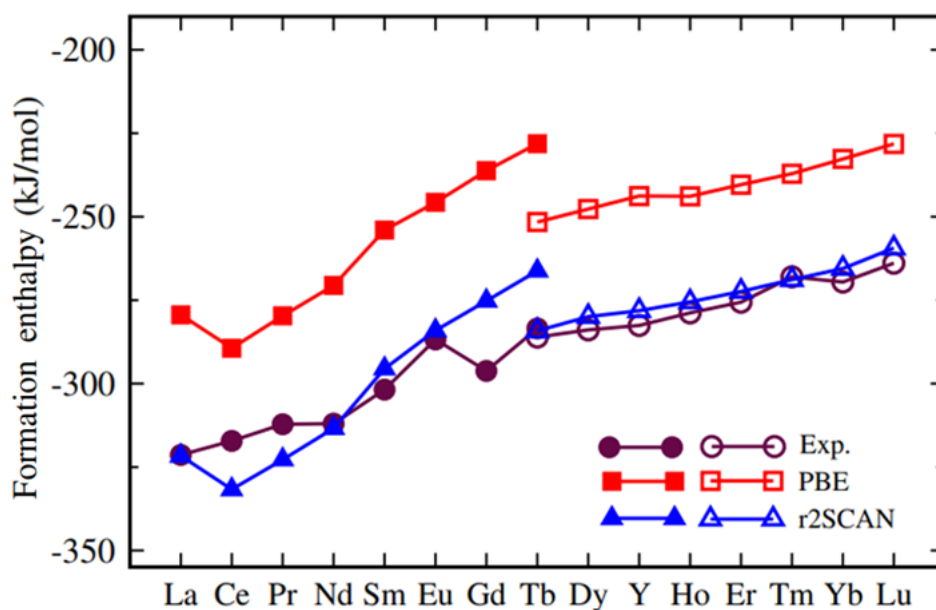


Fig. 3. The formation enthalpies of the monazite (filled symbols) and xenotime (open symbols) rare earth orthophosphates.

3.3 Formation of RE₃PO₇ from RE₂O₃ and REPO₄

Rare earth oxyphosphates have garnered significant research interest due to their promising functional applications in various fields, such as nuclear waste storage, phosphors, and

solid-state lasers [6,7,9,36]. Oxyphosphates like RE_3PO_7 are known for their luminescent properties, particularly when doped with specific rare earth elements like Eu or Tb [9]. This makes them useful in various optical applications, such as LED lighting or display technologies. Additionally, their thermal and chemical stability has led to exploration in catalysis and high-temperature reactions [3]. These compounds feature a network of rare earth cations and phosphate anions, resulting in a structure that can host a variety of functional properties. To date, only a few oxyphosphates (Nd_3PO_7 and Eu_3PO_7) have had their structures experimentally identified as monoclinic ($C2/m$) using single-crystal XRD [4,5]. Y_3PO_7 was found to be isostructural with Gd_3PO_7 , as reported by Tuan et al. [9]. From the MP database [11], four oxyphosphates (La_3PO_7 , Nd_3PO_7 , Sm_3PO_7 , and Tb_3PO_7) are provided with a monoclinic (Cm) symmetry. In our calculations, we used the structures from the MP database and re-optimized the structures for all RE (lanthanides + Y) oxyphosphates. We found that the optimized structures for La_3PO_7 , Ce_3PO_7 , Pr_3PO_7 , and Nd_3PO_7 retain the monoclinic Cm symmetry, while all other RE oxyphosphates exhibit monoclinic $C2/m$ symmetry. The calculated formation enthalpies, based on the reaction in Eq. (2), are presented in Table 5 and Fig. 4. Fig. 4(b) shows the formation enthalpies at 0 K, calculated using the GGA-PBE and r2SCAN exchange-correlation functionals. For all RE_3PO_7 compounds from La through Dy, the formation enthalpies (ΔE_f) are negative, indicating stability against decomposition into oxide and REPO_4 , while other oxyphosphates tend to decompose. Thermal effects on phase stability are not included here and will be discussed below.

Table 5. Calculated total energies and formation enthalpies (in eV/formula unit) for RE_3PO_7 . ΔE_f^M and ΔE_f^X are the formation enthalpy defined in Eq. (2) for the monazite and xenotime REPO_4 , respectively. The value in bold font represents the formation enthalpy for the oxyphosphate RE_3PO_7 , as the calculation uses the most stable REPO_4 phase (also see the filled circles in Fig. 4(a)).

	GGA-PBE			r2SCAN		
	E_{tot}	ΔE_f^M	ΔE_f^X	E_{tot}	ΔE_f^M	ΔE_f^X
La_3PO_7	-90.656	-0.336	-0.459	-178.958	-0.286	-0.528

Ce ₃ PO ₇	-88.876	-0.329	-0.459	-176.725	-0.261	-0.502
Pr ₃ PO ₇	-89.166	-0.332	-0.400	-176.955	-0.269	-0.442
Nd ₃ PO ₇	-89.366	-0.328	-0.339	-177.351	-0.268	-0.378
Sm ₃ PO ₇	-89.576	-0.323	-0.226	-178.765	-0.261	-0.254
Eu ₃ PO ₇	-89.750	-0.316	-0.165	-180.328	-0.243	-0.164
Gd ₃ PO ₇	-89.922	-0.311	-0.110	-182.070	-0.250	-0.116
Tb ₃ PO ₇	-89.975	-0.305	-0.057	-184.066	-0.244	-0.058
Dy ₃ PO ₇	-89.998	-0.294	-0.005	-186.431	-0.237	-0.001
Y ₃ PO ₇	-95.652	-0.263	0.033	-151.144	-0.181	0.055
Ho ₃ PO ₇	-90.012	-0.282	0.046	-189.199	-0.228	0.057
Er ₃ PO ₇	-90.036	-0.270	0.097	-192.447	-0.220	0.112
Tm ₃ PO ₇	-90.109	-0.258	0.149	-196.263	-0.206	0.180
Yb ₃ PO ₇	-90.116	-0.245	0.199	-200.608	-0.196	0.230
Lu ₃ PO ₇	-90.110	-0.238	0.246	-205.210	-0.185	0.291

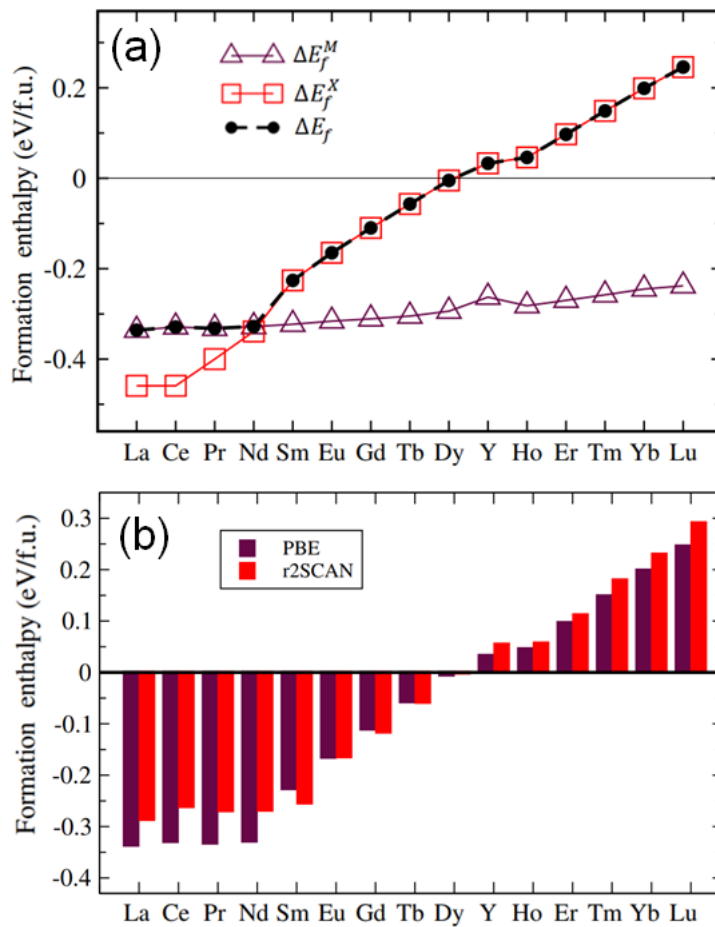


Fig. 4. (a) Illustrating the calculated formation enthalpy ΔE_f (with respect to the most stable

REPO₄ phase and the C-type oxide) for RE₃PO₇ obtained from the formation enthalpies ΔE_f^M and ΔE_f^X . The results are presented for the case of the GGA-PBE exchange-correlation functional. (b) Calculated formation enthalpies ΔE_f using both GGA-PBE and r2SCAN exchange-correlation functionals.

3.4 Vibrational entropy contribution to phase stability

Lattice vibrations are known to have a significant impact on phase stability [37]. The difference in vibrational entropy between phases arises from factors related to atomic and bonding structures, including bond stiffness, volume changes, and atomic size mismatches. The ATAT software [38], developed by Axel van de Walle, provides the *fitfc* method for highly accurate calculations of vibrational free energies. This method fits a Born–von Kármán spring model to the reaction forces generated by imposed atomic displacements in a supercell calculation to determine vibrational properties. The VASP code needs to be invoked to calculate reaction forces for each perturbation. The r2SCAN exchange-correlation functional was employed in the VASP calculations. The *fitfc* calculations were performed for several orthophosphates to investigate the stability of the monazite structure relative to the xenotime structure, as there is a discrepancy between phase stabilities predicted from formation enthalpy calculations at 0 K (Table 3 and Fig. 2) and experimental observations. Figure 5 shows the free energy differences between the monazite and xenotime structures for Nd-, Sm-, Eu-, Gd-, Tb-, Dy-, Ho-, and Y-orthophosphates. It can be seen in Fig. 5 that the monazite phase is preferred for RE orthophosphates up to Sm, while from Dy to Lu (including Y), the xenotime phase is stable. For Eu-, Gd-, and Tb-orthophosphates, both the monazite and xenotime phases may be stabilized in different temperature regions. Therefore, after accounting for the vibrational entropy contribution to free energy, our theoretical predictions of phase stability align more closely with experimental observations.

Formation enthalpy calculations at 0 K have predicted that from Ho to Lu (including Y), the oxyphosphates RE₃PO₇ are unstable and decompose into REPO₄ and RE₂O₃, as shown in reaction Eq. (2). The vibrational entropy contributions at finite temperatures have been calculated by the *fitfc* method for the RE₃PO₇ oxyphosphates with near zero or slightly

positive formation enthalpies at 0 K and Fig. 6 shows the temperature dependence of formation free energy [ΔG_f , calculated by substituting total energies with free energies in Eq. (2)] for those RE_3PO_7 oxyphosphates. After accounting for the vibrational entropy contribution, Y_3PO_7 , Ho_3PO_7 , and Er_3PO_7 can be stabilized at finite temperatures, whereas Tm and later RE oxyphosphates remain unstable below 2200 K. These results, including finite temperature effects, agree well with the experimental observations for RE_3PO_7 phase stability [39].

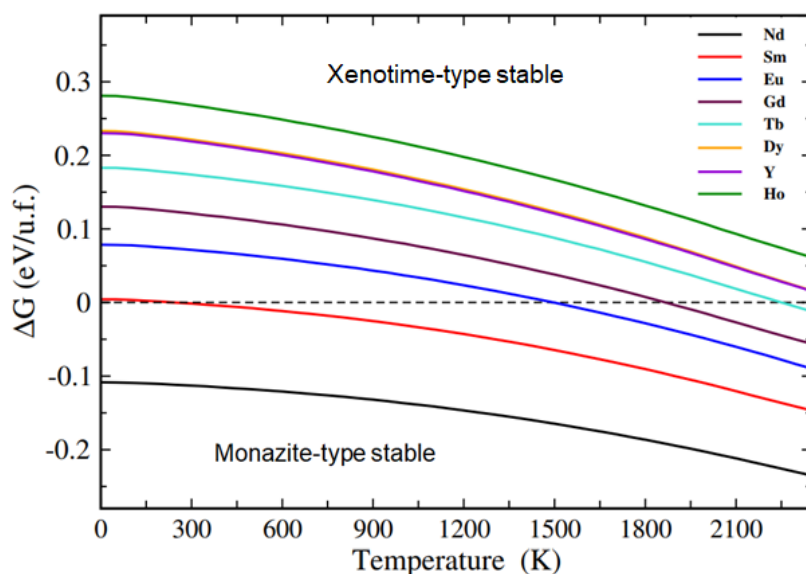


Fig. 5. Free energy difference between the monazite and xenotime phases REPO_4 .

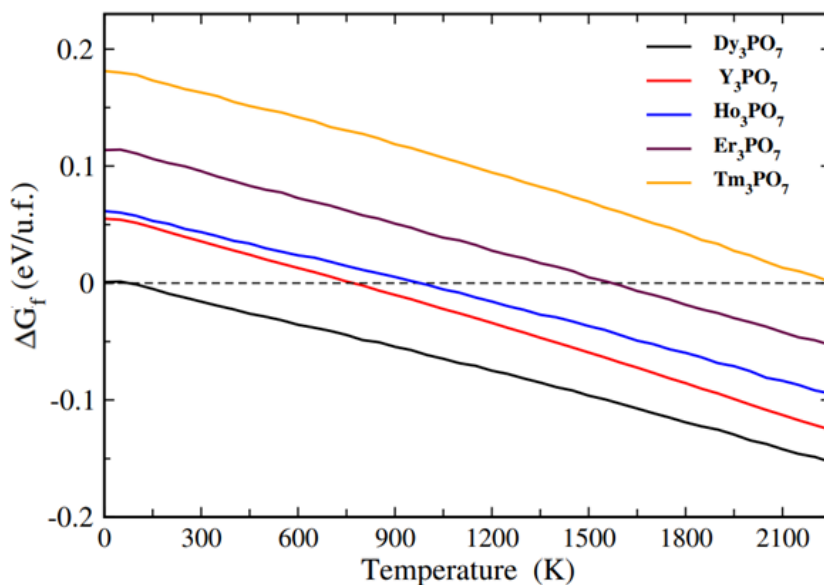


Fig. 6. The dependence of the formation free energy on temperature for oxyphosphates RE_3PO_7 .

5. Conclusions

In conclusion, this study provides a comprehensive computational analysis of the formation enthalpies and phase stability of rare earth phosphates. Both GGA-PBE and r2SCAN functionals predict similar phase stabilities for REPO_4 and RE_3PO_7 , with r2SCAN delivering notably accurate formation enthalpies for monazite and xenotime REPO_4 , closely aligning with experimental results. Including thermal effects, particularly lattice vibrational entropy, further refines free energy predictions, enhancing the agreement between theoretical models and experimental observations on phase stability. These findings underscore the effectiveness of DFT-based methods, particularly with the r2SCAN functional, in accurately characterizing rare earth phosphates' stability and formation properties.

Acknowledgments

This research was supported by US Department of Defense Army Research Office Award number W911NF-23-2-0145, with use of Research Computing at Arizona State University.

References

- [1] J. J. Serra, J. Coutures and A. Rouanet, "Thermal treatment of lanthanide orthophosphates (LnPO_4) and the formation of new (oxyphosphate) compounds," *High Temp. - High Pressures*, vol. 8, p. 337, 1976.
- [2] S. V. Ushakov, "Rare earth oxyphosphates: Pressure-temperature constraint for impact melts?," *Geological Society of America Abstracts with Programs*. Vol. 56, No. 5, 2024, vol. 56, 2024.
- [3] S. N. Achary, S. Bevara and A. K. Tyagi, "Recent progress on synthesis and structural aspects of rare-earth phosphates," *Coordination Chemistry Reviews*, vol. 340, p. 266–297, 2017.
- [4] W. Grunwald, K. Wittich and R. Glaum, "Anhydrous Europium Phosphates: A Comprehensive Report on Syntheses, Crystal Structures, and Phase Relations," *Z. Anorg. Allg. Chem.*, vol. 644, p. 1403–1414, 2018.
- [5] K. K. Palkina, N. E. Kuz'mina, B. F. Dzhurinskii and E. G. Tselebrovskaya, *Dokl. Akad. Nauk*, vol. 341, p. 644–648, 1995.
- [6] M. S. Wong and E. R. Kreidler, "Phase Equilibria in the System $\text{Nd}_2\text{O}_3\text{-P}_2\text{O}_5$," *J. Am. Ceram. Soc.*, vol. 70, pp. 396-399, 1987.
- [7] N. Hatada, T. Nagai, Y. Nose and T. Uda, "Reinvestigation of the phase equilibria in the $\text{La}_2\text{O}_3\text{-P}_2\text{O}_5$ system," *Journal of Phase Equilibria and Diffusion*, vol. 34, pp. 196-201, 2013.
- [8] D. Agrawal and F. A. Hummel, "The Systems $\text{Y}_2\text{O}_3\text{-P}_2\text{O}_5$ and $\text{Gd}_2\text{O}_3\text{-P}_2\text{O}_5$," *J. Electrochem. Soc.*, vol. 127, p. 1550, 1980.
- [9] D. C. Tuan, R. Olazcuaga, F. Guillen, A. Garcia, B. Moine and C. Fouassier,

- "Luminescent properties of Eu^{3+} -doped yttrium or gadolinium phosphates," *J. Phys. IV France* , vol. 123, p. 259–263, 2005.
- [10] S. V. Ushakov, K. B. Helean and A. Navrotsky, "Thermochemistry of rare earth orthophosphates," *Journal of Materials Research*, 16, 2623–2633, 2002.
- [11] A. Jain, S. P. Ong, G. Hautier, W. Chen, W. D. Richards, S. Dacek, S. Cholia, D. Gunter, D. Skinner, G. Ceder and K. A. Persson, "Commentary: The Materials Project: A materials genome approach to accelerating materials innovation," *APL Mater.* , vol. 1, p. 011002, 2013.
- [12] P. Hohenberg and W. Kohn, "Inhomogeneous Electron Gas," *Phys. Rev.*, vol. 136, p. B864, 1964.
- [13] W. Kohn and L. J. Sham, "Self-consistent equations including exchange and correlation effects," *Physical Review.*, vol. 140, p. A1133–A1138, 1965.
- [14] N. Marzari, A. Ferretti and C. Wolverton, "Electronic-structure methods for materials design," *Nature Materials*, vol. 20, pp. 736-749, 2021.
- [15] J. P. Perdew, K. Burke and M. Ernzerhof, "Generalized Gradient Approximation Made Simple," *Phys. Rev. Lett.*, vol. 77, pp. 3865-3868, 1996.
- [16] J. W. Furness, A. D. Kaplan, J. Ning, J. P. Perdew and J. Sun, "Accurate and Numerically Efficient r2SCAN Meta-Generalized Gradient Approximation," *J. Phys. Chem. Lett.*, vol. 11, p. 8208–8215, 2020.
- [17] G. Kresse and J. Furthmüller, "Efficiency of ab-initio total energy calculations for metals and semiconductors using a plane-wave basis set," *Comp. Mater. Sci.*, vol. 6, pp. 15-50, 1996.
- [18] G. Kresse and J. Furthmüller, "Efficient Iterative Schemes for Ab Initio Total-Energy

- Calculations Using a Plane-Wave Basis Set," *Phys. Rev. B*, vol. 55, pp. 11169-11174, 1996.
- [19] P. Blöchl, "Projector augmented-wave method," *Phys. Rev. B*, vol. 50, pp. 17953-17979, 1994.
- [20] "https://www.vasp.at/wiki/index.php/Available_pseudopotentials," [Online].
- [21] R. Kingsbury, A. S. Gupta, C. J. Bartel, J. M. Munro, S. Dwaraknath, M. Horton and K. A. Persson, "Performance comparison of *r2SCAN* and *SCAN* metaGGA density functionals for solid materials via an automated, high-throughput computational workflow," *Phys. Rev. Materials*, vol. 6, p. 013801, 2022.
- [22] M. Kothakonda, A. D. Kaplan, E. B. Isaacs, C. J. Bartel, J. W. Furness, J. Ning, C. Wolverton, J. P. Perdew and J. Sun, "Testing the *r2SCAN* density functional for the thermodynamic stability of solids with and without a van der Waals Correction," *ACS Mater. Au*, vol. 3, p. 102–111, 2023.
- [23] J. Sun, A. Ruzsinszky and J. P. Perdew, "Strongly constrained and appropriately normed semilocal density functional," *Phys. Rev. Lett.*, vol. 115, p. 036402, 2015.
- [24] J. P. Perdew, A. Ruzsinszky, G. I. Csonka, O. A. Vydrov, G. E. Scuseria, L. A. Constantin, X. Zhou and K. Burke, "Restoring the density-gradient expansion for exchange in solids and surfaces," *Phys. Rev. Lett.*, vol. 100, p. 136406, 2009.
- [25] H. J. Monkhorst and J. D. Pack, "Special points for Brillouin-zone integrations," *Phys. Rev. B*, vol. 13, pp. 5188-5192, 1976.
- [26] C. J. Bartel, "Review of computational approaches to predict the thermodynamic stability of inorganic solids," *J. Mater. Sci.*, vol. 57, p. 10475–10498, 2022.
- [27] Y. Zhang and I. Jung, "Critical evaluation of thermodynamic properties of rare earth

- sesquioxides (RE = La, Ce, Pr, Nd, Pm, Sm, Eu, Gd, Tb, Dy, Ho, Er, Tm, Yb, Lu, Sc and Y)," *Calphad*, vol. 58, pp. 169-203, 2017.
- [28] S. Atkinson, Crystal structures and phase transitions in the rare earth oxides. (Thesis). University of Salford, 2014.
- [29] J. R. Rustad, "Density functional calculations of the enthalpies of formation of rare-earth orthophosphates," *American Mineralogist*, vol. 97, p. 791–799, 2012.
- [30] E. A. Kummerle and G. Heger, "The Structures of $C-Ce_2O_{3+\delta}$, Ce_7O_{12} , and $Ce_{11}O_{20}$," *Journal of Solid State Chemistry*, vol. 147, pp. 485-500, 1999.
- [31] E. Shoko, M. F. Smith and R. H. McKenzie, "Mixed valency in cerium oxide crystallographic phases: Valence of different cerium sites by the bond valence method," *PHYSICAL REVIEW B*, vol. 79, p. 134108, 2009.
- [32] A. B. Romero, P. M. Kowalski, G. Beridze, H. Schlenz and D. Bosbach, "Performance of DFT+U Method for Prediction of Structural and Thermodynamic Parameters of Monazite-Type Ceramics," *Journal of Computational Chemistry*, vol. 35, pp. 1339-1346, 2014.
- [33] G. Beridze, A. Birnie, S. Koniski, Y. Ji and P. M. Kowalski, "DFT+U as a reliable method for efficient ab initio calculations of nuclear materials," *Progress in Nuclear Energy*, vol. 92, pp. 142-146, 2016.
- [34] Y. Ji, P. M. Kowalski, P. Kegler, N. Huittinen, N. A. Marks, V. L. Vinograd, Y. Arinicheva, S. Neumeier and D. Bosbach, "Rare-Earth Orthophosphates From Atomistic Simulations," *Front. Chem.*, vol. 7, p. 197, 2019.
- [35] S. Chong, B. J. Riley, X. Lu, J. Du, T. Mahadevan and V. Hegde, "Synthesis and properties of anhydrous rare-earth phosphates, monazite and xenotime: a review," *RSC*

Adv., vol. 14, p. 18978–19000, 2024.

- [36] T. S. Dhapodkar¹, A. R. Kadam, A. Duragkar, N. S. Dhoble and S. JDhoble, "Recent progress in phosphate based luminescent materials: A case study," *Journal of Physics: Conference Series*, vol. 1913, p. 012024, 2021.
- [37] A. van de Walle and G. Ceder, "The Effect of Lattice Vibrations on Substitutional Alloy Thermodynamics," *Rev. Mod. Phys.*, vol. 74, pp. 11-45, 2002.
- [38] A. van de Walle, "Multicomponent multisublattice alloys, nonconfigurational entropy and other additions to the Alloy Theoretic Automated Toolkit," *CALPHAD: Computer Coupling of Phase Diagrams and Thermochemistry*, vol. 33, pp. 266-278, 2009.
- [39] S. V. Ushakov et al, "Rare earth oxyphosphates – review," To be published, 2024.